Micro-assembly and modeling of the liquid microworld: the PRONOMIA project

M.Gauthier[1], S. Régnier[2], B. Lopez-Walle[1], E. Gibeau[1], P. Rougeot[1], D. Hériban[1], N. Chaillet[1].

[1]Laboratoire d'Automatique de Besançon
CNRS - ENSMM - UFC
24, rue Alain SAVARY
25000 Besançon (France)
gauthier@ens2m.fr

[2]Laboratoire de Robotique de Paris
CNRS - UPMC
BP 61
92265 Fontenay Aux Roses (France)
regnier@robot.jussieu.fr

***Abstract*— This paper presents an overview of the French research program PRONOMIA which deals with new methods for robotic micromanipulation and especially on submerged micromanipulation. During microscale object manipulation, contact (pull-off) forces and non-contact (capillary, van der Waals, and electrostatic) forces determine the behavior of the micro-objects rather than the inertial forces. This article introduces a review of the major differences between dry and submerged micromanipulations and gives an experimental analysis of the physical phenomena at a microscopic scale in dry and liquid media. New submerged microhandling strategies is necessary to perform micromanipulation in a liquid. Two solutions are proposed in this article which use a freeze gripper and a dielectrophoretic gripper. Finally, microassembly and biological applications are presented.**

Keywords: **Microassembly, liquid medium, microforce modeling, microforce measurement, handling strategies.**

I. Introduction

The complexity of the microsystems is always higher and requires a lot of different materials and different microfabrication processes. Without micro-assembly technologies, it is more and more difficult to build microsystems and especially optical microsystems [1]. Consequently, the advent of new hybrid microsystems requires new micro-assembly technologies and methods. There are two main approaches in this domain: Self-assembly and robotic assembly. The first approach is useful for a very large production batch but the reliability stays low [2]. The second approach is more flexible and is relevant for a smaller production batch [3], [4].

Robotic micro-assembly tasks require firstly to be able to manipulate (to catch, to position, to release) microscopic objects whose typical size is included between one millimeter and one micrometer (micromanipulation).

The physical scale of micromanipulation is near to the lower limit of traditional mechanics. In general, the laws of Newtonian physics are still valid and the quantum effects neglected: The scale considered is thus at the boundary of two traditional spaces whose limits are not exactly known. The major difference with the macroscopic scale is indeed the results from the considered forces. The volume forces are negligible in respect to the surface forces for the microscopic objects [5-8]. These forces, whose effects are negligible on a macroscopic scale, modify drastically the contact mechanics and the interactions between the various media.

These surface forces may affect the micromanipulation task and especially the release of the micro-object. The frontier generating the modification of the micro-object behavior (from a behavior dominated by surface forces rather than volume based forces) is a function of the material of the micro-gripper, object, and the surrounding medium. In most cases, this frontier corresponds to the specific dimension of the micro-object near 100 micrometers, and at the present time, no repeatable and reliable micromanipulator exists under this physical limit.

Most modeling of the micro-world is done in the dry medium (air or vacuum) [7], [9]. The liquid medium is not studied even through it could have a lot of advantages in micromanipulation of artificial objects under the limit of 100 micrometers. The objective of this work is to present the potential advantages of the liquid in artificial micro-object micromanipulation by means of theoretical and experimental forces analysis and first comparative pushing micromanipulations.

This article focuses on the theoretical and experimental comparison between both types of medium. However we focus this article on the experimental and theoretical analysis on micromanipulations in water, our general approach concerns liquids and not only water. The aim of to propose an overview on the advantages and drawback of the submerged micro-assembly.

The following section focuses on the theoretical impact of the medium on distance forces (van der Waals, electrostatic, capillary forces), contact forces (pull-off forces) and hydrodynamic forces . Thereafter, the measurements of distance and contact forces are presented and compared to theoretical values. Innovative submerged handling strategies is also proposed. The last

section deals with applications in microassembly and biological application.

II. Theoretical Analysis

A lot of studies have been carried out on forces at microscopic scale. They use either classical models of forces at microscopic or nanoscopic scale (van der Waals, capillary, electrostatic forces) or theories of macroscopic contact (Hertz, JKR or DMT models). We propose a general approach by sorting out these forces considering the distinction whether there is contact or not. When there is no physical contact between two solids, the forces in action are called distance forces. According to the scientific literature in this domain [8], [10], [11], the latter are electrostatic, van der Waals and capillary forces. In case of water medium, hydrophobic forces, steric forces and double-layer forces have to be considered too. When two solids are in contact, some object deformation appear which induce adhesion forces in the contact surface. In this case, we consider contact forces (usually denoted pull-off forces). Electrostatic or capillary effects can be added, but van der Waals forces are not considered anymore, because they are already involved in the pull-off term. In liquid the hydrodynamic effects have to be considered. Thus, the third type of forces presented is the hydrodynamic forces [12].

A. Surface Forces

1) Van der Waals Forces: The van der Waals forces are a well-known interatomic interaction forces. For an interaction between a flat substrate (1) and a spherical object (2), the integrated van der Waals force is equal to:

$$F_{vdw}(D) = -\frac{A_{12}R}{6D^2} \tag{1}$$

where A_{12} is the Hamaker constant of the interaction (1-2), D is the contact distance between (1) and (2) and R is the radius of the spherical object (2).

Parameter A_{12} usually takes values included in the interval $[0.4-4]\times10^{-19}$J [12-15]. It is possible to obtain approximated values of A_{12} by using the "combination laws", derived from the expression of A_{12} introduced by Mac Lachlan in 1963 [17]: For two materials interacting in vacuum, A_{12} is computed according to the constants A_{ii} of each material:

$$A_{12} \simeq \sqrt{A_{11}A_{22}} \tag{2}$$

The Hamaker constant could be determined through the Lifshitz-van der Waals constant too [18]:

$$A_{12} = \frac{3H_{LV}}{4\pi} \tag{3}$$

where H_{LV} is the Lifshitz-van der Waals constant.

For interaction of two materials in the presence of a third medium (3), the total force F_t to considered is expressed by the extended DLVO theory (XDLVO) proposed by Xu and Yoon [19], [20]:

$$F_t = F_{vdw} + F_{dl} + F_h \tag{4}$$

The total force is the sum of the van der Waals force, the double-layer force and a third term which represents all other forces except van der Waals force and double-layer force, such as solvation, structural, hydration, hydrophobic, steric, fluctuation forces, etc.
The van der Waals force in a third medium is a function (1) of the Hamaker constant denoted A_{132} estimated by:

$$A_{132} = A_{12} + A_{33} - A_{13} - A_{23} \tag{5}$$

Consequently, from (2), A_{132} verifies:

$$A_{132} =\simeq (\sqrt{A_{11}} - \sqrt{A_{33}})(\sqrt{A_{22}} - \sqrt{A_{33}}) \tag{6}$$

The repulsive double layer force F_{dl} can be currently written as [15], [21], [22]:

$$F_{dl} \simeq 4\pi R\epsilon_3\kappa_3\Phi_1\Phi_2 e^{-\kappa_3 D} \tag{7}$$

where ϵ_3 is the dielectric constant of the medium, Φ_1 and Φ_2 are the surface potentials of the sphere and the surface and κ_3 the Debye length of the medium. The repulsive double layer force F_{dl} is typically greater than the van der Waals force between $D = 1\,nm$ to $D = 10 - 20\,nm$ [15]. This repulsive force is able to reduce the impact of the van der Waals force in this range.
The third term represents notably the solvation forces which have typically significant impact at very small range lower than $10\,nm$. In water, these forces are repulsive for hydrophilic surface and attractive for hydrophobic surface [15]. In case of hydrophilic surface these forces are able to reduce the impact of the van der Waals force.

Table I gives the values of Hamaker constant for some materials in vacuum and in water. The immersion is then able to reduce the value of the van der Waals force. However, this force has a short range (typically $< 100\,nm$) compared to the size of the object (greater than $1\,\mu m$). The impact of this force on the micro-objects behavior is thus limited compared to the very long range of electrostatic interaction and contact forces.

Materials	**Vacuum**	**Water**
Gold	40	30
Silver	50	40
Al_2O_3	16.8	4.4
Copper	40	30

TABLE I
Values of Hamaker constant for some materials
$A \times 10^{-20} J$ [23]

2) Electrostatic Forces: The force applied by an electrostatic surface (σ surface charge density) on an electric charged particle (q) is given by:

$$F_e = \frac{q\sigma}{2\varepsilon_0\varepsilon} \tag{8}$$

where ε and ε_0 are respectively the relative dielectric constant of the medium and the dielectric constant of the vacuum.

Comparison of dielectric constants between the water and the air is presented in Table II. The water dielectric constant is more important than the air dielectric constant. So, in the same electrical charges configuration (q, σ) electrostatic force is significantly reduced in water.

Moreover electrostatic perturbations observed in micromanipulation are caused by tribo-electrification. During a micro-assembly task, friction between manipulated objects induces electric charges on surface of the objects. The charge density depends on the tribo-electrification and conductivity of the medium. Effectively, a higher electric conductivity medium is able to discharge objects surfaces. The water, especially ionic water, has better electric conductivity than the air (Table II). Consequently, charge density in water is reduced. The electrostatic force directly proportional to the charge density σ is therefore reduced.

Electric parameters	**Air**	**Water**
Dielectric constant ε	~ 1	80.4
Conductivity	$10^{-7}\, S.m^{-1}$	$> 10^{-4}\, S.m^{-1}$

TABLE II
RELATIVE DIELECTRIC CONSTANT AND ELECTRICAL CONDUCTIVITY OF AIR AND WATER

Both impacts of the immersion on electric properties of the medium (dielectric constant and conductivity) induce a reduction of electrostatic forces. In conclusion, electrostatic perturbations are highly reduced in water compared to the air.

3) Capillary Forces: Basically, the capillary forces arise in two ways: Either a liquid drop is put between two solids (e.g. a gripper and a component) that turns itself towards a meniscus (a liquid bridge), or a capillary bridge appears by condensation of the ambient humidity in the small cracks and pores made by two rough profiles brought together in contact.

In both cases, the situation can be described by a liquid bridge presented in Figure 1 characterised by a volume V, a liquid surface tension γ and wettability properties defined by the contact angles θ_1 and θ_2. Most often the capillary forces are approximated by several formulations. With the assumptions that the contact angles are equal $\theta_1 = \theta_2 = \theta$, a constant volume and immersion height (D) is small, capillary force between a plan and sphere (radius R) is equal to [15]:

$$F_c = \frac{4\pi R\gamma\cos\theta}{1 + (D/d)} \tag{9}$$

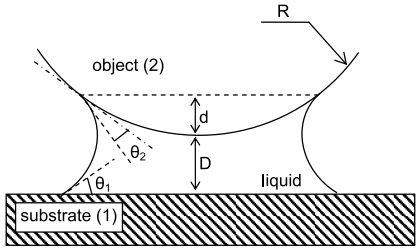

Fig. 1. Liquid meniscus formation between a spherical object and a substrate.

This capillary force is induced by the surface between the liquid and the air near to the object. In liquid this surface disappears, so this force is canceled in liquid medium. However, capillary force appears in the interface between the liquid and the air. This force is able to perturb end-effectors behavior and micro-object immersion. A complete study of the impact of capillary force on submerged micromanipulations is proposed in [24].

B. Contact Forces

The pull-off force represents the force necessary to break the contact surface between two objects. In case of a sphere (radius R) on a planar surface, pull-off force P is approximately given by JKR[1] (for the lower boundary) or DMT[2] (for the higher boundary) contact models [25], [26]:

$$\frac{3}{2}\pi R W_{12} \leq P \leq 2\pi R W_{12} \tag{10}$$

where W_{12} is the work of adhesion between both objects (1) and (2).

In the air, the work of adhesion is expressed by [27]:

$$W_{12} = \gamma_1 + \gamma_2 - \gamma_{12} \simeq 2\sqrt{\gamma_1\gamma_2} \tag{11}$$

where γ_{12} is the interfacial energy and γ_1, γ_2 are the surface energy of both objects.

According to [28], the Maugis elasticity parameter λ can be used to choose the most appropriate contact model for a given case. This parameter is expressed for an interface between two bodies (1) and (2) with:

$$\lambda = 2\sigma_0 \left(\frac{R}{\pi W_{12} K^2}\right)^{\frac{1}{3}} \tag{12}$$

$$\tag{13}$$

where K is the equivalent elastic modulus, calculated using the both Poisson's ratios μ_1, μ_2 and both Young's modulus E_1, E_2:

$$K = \frac{4}{3}\left(\frac{1-\mu_1^2}{E_1} + \frac{1-\mu_2^2}{E_2}\right)$$

[1]Johnson, Kendall and Roberts [25]
[2]Derjaguin, Muller and Toporov [26]

The parameter σ_O is defined by:

$$\sigma_0 = \frac{W_{12}}{h} \tag{14}$$

where $h \simeq 10^{-10} m$.

Using λ, the pull-off force can be estimated with:

$$\begin{aligned} \lambda < 0.1 &\implies \text{DMT model: } P = 2\pi R W_{12} \\ \lambda > 5 &\implies \text{JKR model: } P = \tfrac{3}{2}\pi R W_{12} \\ 0.1 < \lambda < 5 &\implies \text{Dugdale model:} \\ & P = \left(\tfrac{7}{4} - \tfrac{1}{4}\tfrac{4.04\lambda^{\frac{1}{4}}-1}{4.04\lambda^{\frac{1}{4}}+1}\right)\pi R W_{12} \end{aligned} \tag{15}$$

Moreover, in case the objects are submerged in medium (3), the surface energy, denoted W_{132}, required to separate two objects (1) and (2) submerged in a medium 3 is given by:

$$W_{132} = W_{12} + W_{33} - W_{13} - W_{23} \simeq \gamma_{13} + \gamma_{23} - \gamma_{12} \tag{16}$$

For example, in case of a SiO_2-SiO_2 contact ($\gamma_{SiO_2} = 290\ mJ.m^{-1}$ [23]), the theoretical surface energies in air and in water are (from (11), (16)):

$$W_{12} = 580\ mJ.m^{-1} \quad W_{132} = 146\ mJ.m^{-1} \tag{17}$$

In this example, the pull-off force is reduced in water compared to the air. Usually, solid state surface energies are around $1000\, mJ.m^{-1}$ and the theoretical pull-off reduction is around 50% to 80%.

C. Impact of the Hydrodynamic Forces on the Micro-objects Behavior

In this section the impact of the hydrodynamic forces on the behavior of micro-objects is described. In the micro-world, the Reynolds number which characterizes the liquid flow is usually very low (< 1). The flow is thus highly laminar. In case of a micro-object placed in an uniform liquid flow, the Stokes law directly gives the hydrodynamic force applied on the object. This law is valid when the flow Reynolds number is lower than 1 and can be extrapolated to Reynolds number lower than 10 with a good approximation.
The Stokes law defines the force applied on an object in a uniform flow of fluid defined by a dynamic viscosity μ and a velocity V:

$$\overrightarrow{F}_{hydro} = -k.\mu.\overrightarrow{V} \tag{18}$$

where k is a function of the geometry. In case of a sphere with a radius R, k is defined by

$$k = 6\pi R$$

Table III gives the values of dynamic viscosity μ of both water and air. Then the hydrodynamic force proportional to the dynamic viscosity highly increases in a submerged medium.

As inertial effects are very small in the micro-world, micro-objects accelerations are usually very high. In this way, micro-object velocity is able to increase in a very short time. Consequently, micro-objects can reach high velocity, and object trajectory could be difficult to control especially in case of a visual feedback. In fact, the object can jump rapidly out of the field of view and this induces its loss. So, in most cases, velocity limitation in the submerged micro-world does not depend on inertial physical limitation but on hydrodynamic physical limitation. From this, a liquid medium is able to reduce maximal micro-objects velocity [29]. Consequently, the increasing of hydrodynamic force is able to limit the maximal velocity of the objects and thus significantly reduces the loss of micro-objects.

Dynamic viscosity	**Water**	**Air**
$\mu\ [kg.m^{-1}.s^{-1}]$	10^{-3}	$18.5\,10^{-6}$

TABLE III
DYNAMIC VISCOSITY OF WATER AND AIR, $T^{\circ} = 20^{\circ}C$

However, movements of liquid induced by the movement of the effector are able to lead to significant hydrodynamic force on micro-objects. Consequently the hydrodynamic force induces a limitation of the maximum velocity of the effector to avoid disturbance on the micro-object position. Nevertheless, experimentally the maximum velocity of the effector can stay high (eg. $1\, mm.s^{-1}$) compared to the typical size of the object manipulated ($50\, \mu m$).

In conclusion, contact, non contact and hydrodynamic force were presented in both liquid and dry media. This analysis shows the reduction of contact and non contact forces in liquid compared to the air. As these effects are able to perturb the micromanipulation tasks, the use of a liquid could improve the efficiency of micromanipulation. Moreover, the increase of the hydrodynamic effects are beneficial on the micro-objects behavior during their micromanipulation. Thus, the theoretical study shows the interest of submerged media for such tasks.

III. FORCES MEASUREMENT

To analyse the validity of the micro-force modeling, some experimental force measurements are necessary. This part deals with the presentation of the micro-force measurement device and the comparison between theoretical and experimental values.

A. AMIS System

The micro-forces are measured by a specifically developed system called *AMIS* (AFM based MIcromanipulation System). This system is based on a standard Atomic Force Microscope (AFM) and a 3D micromanipulation system which allows large displacement (which is not usually the case in a standard AFM). In particular, AMIS is used to study the pull-off force. Experiments were carried out with polystyrene (PS) and glass substrates.

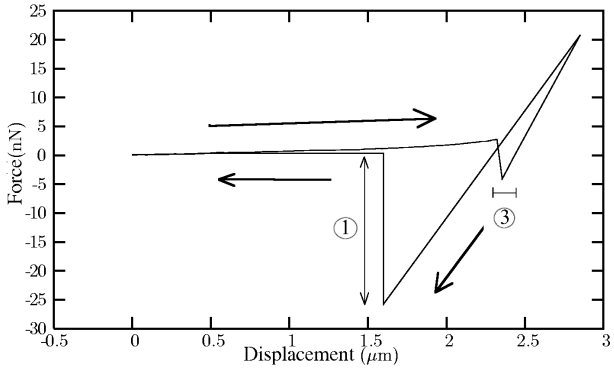

(a) Interactions between AFM tip and a PS substrate.

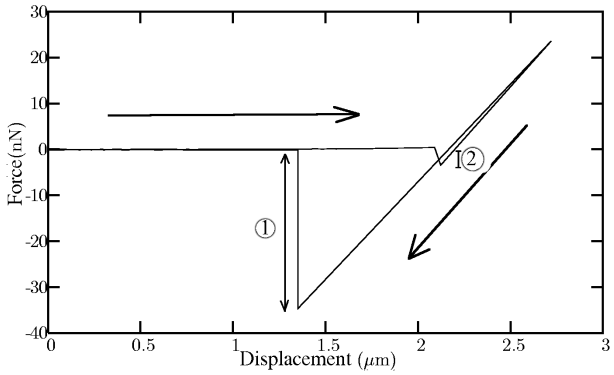

(b) Interactions between AFM tip and a glass substrate.

Fig. 2. Force-distance curves in air.

The pull-off force is measurable on the experimental force-distance curves when the breaking load between the AFM tip and the substrate appears (mark (1) in the Figure 2). From these curves (Figure 2), an experimental value of the pull-off forces for both interactions is measured. These values are estimated as:

$$P^{\text{measured}}_{\text{silicon-PS}} = 26\ nN \tag{19}$$

$$P^{\text{measured}}_{\text{silicon-glass}} = 35\ nN \tag{20}$$

From equation (11), (12), (15) and physical properties described Table IV, theoretical pull-off forces can be calculated:

$$P_{\text{silicon-PS}} = 28\ nN \quad (\lambda = 0.33\ ) \tag{21}$$

$$P_{\text{silicon-glass}} = 49\ nN \quad (\lambda = 0.54\ ) \tag{22}$$

These values (21)-(22) fit very closely to the measurements (19)-(20). Hence, theoretical estimation of pull-off forces can generally be trusted when no direct measurements are possible.

In order to analyse the influence of the environment, pull-off force measurement was done in aqueous medium. Figure 3 describes the force-distance curve of a silicon-glass interface in water. The experimental pull-off force is thus estimated as:

$$P^{\text{measured}}_{\text{silicon-water-glass}} = 5.5\ nN \tag{23}$$

From equation (16), (12), (15) and physical properties described Table IV, theoretically calculated pull-off force is then:

$$P_{\text{silicon-water-glass}} = 16.0\ nN \tag{24}$$

Pull-off force induces adhesion effects in a micromanipulation task. Consequently the significant reduction of the pull-off force in liquid is able to reduce adhesion perturbations in submerged micromanipulations.

Material	γ	A	ν	E
Unity	mJ.m^{-2}	$\times 10^{-20}$ J	-	GPa
Silicon	1400	26	0.17	140
Polystyrene (PS)	36	7.9	0.35	3.2
Glass	170	6.5	0.25	69

TABLE IV

Physical properties of the materials used in the experiments.

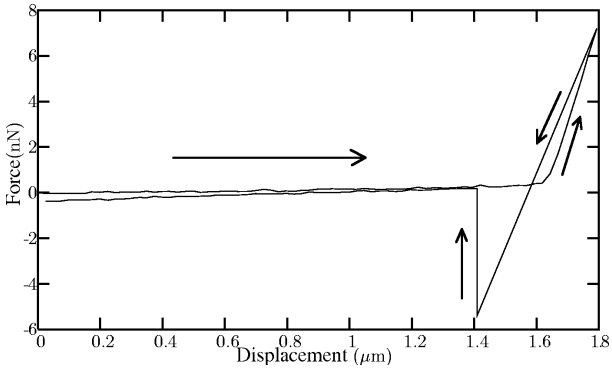

Fig. 3. Force-distance curve for an interaction between the cantilever and a glass substrate in an aqueous medium.

1) Electrostatic Forces: This part deals with the electrostatic forces in case of contact with conductors and insulators. AFM tip is made of silicon and is grounded. The first experiment describes a contact with a gold substrate (Figure 4). Comparative electrostatic force measurements were done on grounded and non grounded gold surface. These experimentations clearly show that the electrostatic force (marks 2 in Figure 4) is reduced when the substrate is grounded. On a non grounded substrate, the electrostatic forces appears at a very significant separation distance (mark 1 in Figure 4a) compared to the other forces (ten micrometers).

The second study is led on an insulator, PS substrate. The results are done in Figure 5. In the same way, to avoid this force, the substrate is cleaned with distilled water. The curve obtained is then represented on the Figure 5b. The electrostatic force is clearly reduced after charge cleaning (marks 2 in figure 5). In the first case, the interaction distance of the

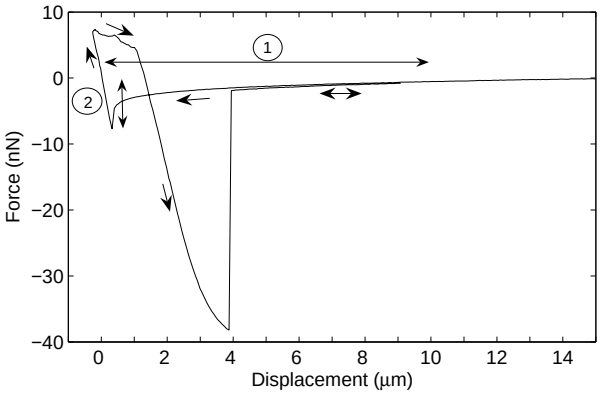

(a) Non grounded substrate.

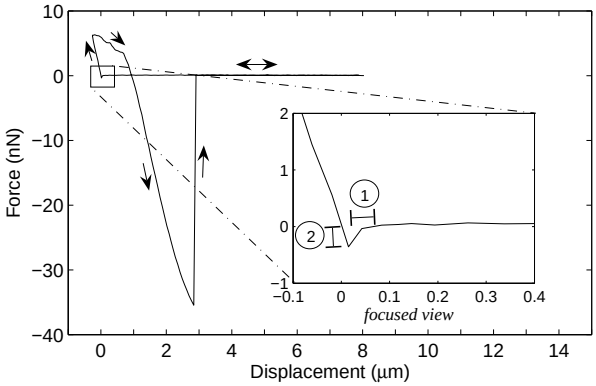

(b) Grounded substrate.

Fig. 4. Force-distance curves in air with a gold substrate.

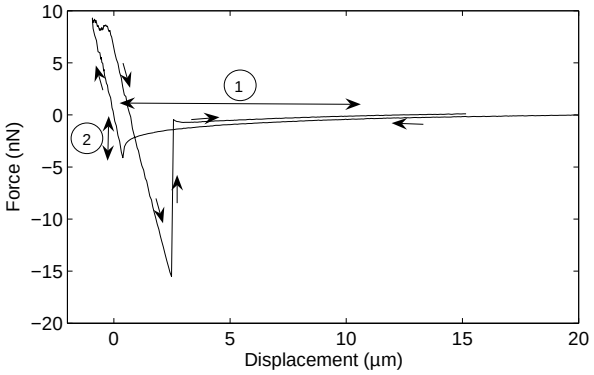

(a) Substrate without charges cleaning.

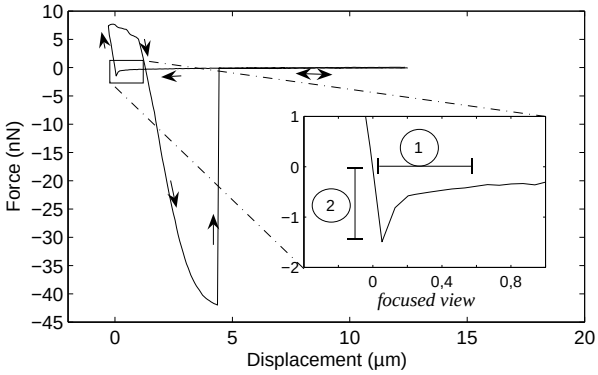

(b) Substrate after cleaning the substrate with distilled water.

Fig. 5. Force-distance curves with a polystyrene substrate.

electrostatic (marks 1 in figure 5a) which is about ten micrometers is larger than the interaction distance of the other forces again. The modification of the pull-off force between both cases presented figure 5 has not been studied. It could be explained by capillary forces induced by residual water after cleaning.

To illustrate electrostatic perturbations, a third experimental study was done: The approach of the AFM cantilever with a copper substrate initially charged with a 2 V voltage. The approach curve of the AFM cantilever is then drastically modified (see Figure 6). The cantilever is periodically attracted by the substrate and release due to electrostatic effects. The attraction is induced by the long range of the electrostatic forces while the release is obtained by a local discharge of the substrate induced by the contact with the micro-tip. Moreover, tip effects can be observed, making difficult any identification. In the same way, this phenomenon disappears as soon as the substrate is grounded.

Electrostatic forces are efficient in long range, starting at 10 μm and have the highest modules of the distance forces. As the charge density of a micro-object is not exactly known, the values of the electrostatic forces in a real system are hard to model. The reduction of the electrostatic perturbations is thus a key point to perform repeatable and precise micromanipulations. In dry medium, the cancellation of electrostatic effects can be obtained by grounding for conductor or by using distilled water for insulator. In liquid, i.e water, the electrostatic effects are highly reduced (section II-A.2). In fact, no electrostatic forces were measured in water.

The force measurements performed with the AMIS device prove a relatively good correlation between the micro-force models and the experimental forces. Moreover, the advantages of the liquid presented in section II, is confirmed by the experimental forces measurement.

In conclusion, the measurements of the non contact and contact forces generally show a good correlation between the theoretical models and the experiments. The correlation between the theoretical forces and the measured forces is better than 40% (except for pull-off in water). The measurement of the reduction of the pull force in water, and the cancellation of the electrostatic perturbations confirm the theoretical analysis. The interest of the submerged micromanipulation is thus

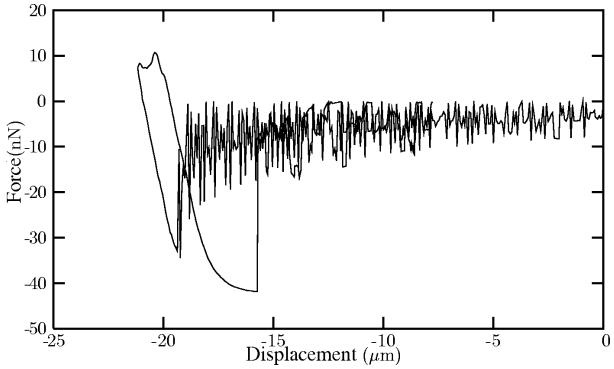

Fig. 6. Electrostatic perturbations measured by AMIS.

confirmed by the force measurements.

IV. Submerged Microhandling Strategies

Though the adhesion forces are reduced in liquid, sticking effects are not totally canceled[12] and the release task stays a critical problem. Thus the study of new release strategies of artificial micro-objects in liquid is a key-point to perform submerged micro-assembly. As current microhandling strategies of artificial objects are performed in the air (or vacuum), new micromanipulation strategies are required to manipulate in the liquid. Two ways can be explored:

- strategies based on principles used in biomicromanipulation. In this case, principles can be improved or modified to be able to handle artificial objects in spite of biological objects (no more biocompatibility, more degree of freedom required...);
- new strategies, currently not use in liquid because of biological constraints.

One example of each ways is presented in the following : a dielectrophoretic gripper and a freeze gripper.

A. Dielectrophoretic Gripper

In the current micromanipulations, usual approaches consist in control of a repulsive physical force to overcome the pull-off force (eg. acceleration in air [30]). We propose to use repulsive dielectrophoretic force to overcome pull-off force to control the release of the micro-objects. This principle usually used in biological cell manipulations is easily controllable by an electric field and is particularly efficient in liquid.

1) Principle of Dielectrophoresis: The time averaged dielectrophoretic force F_{DEP} and torque T_{DEP} applied by a particle in an inhomogeneous electric field $\vec{E}(t)$ is expressed by [31]:

$$\vec{F}_{DEP} = K_g.K_{DEP}.\epsilon_3.\vec{\nabla}E(rms)^2 \quad (25)$$

$$\vec{T}_{DEP} = K_g.K'_{DEP}.\epsilon_3.(E_x^2 \bigtriangledown \phi_x + E_y^2 \bigtriangledown \phi_y + E_z^2 \bigtriangledown \phi_z) \quad (26)$$

where $E(rms)$ is the rms value of the electric field strength, E_i and ϕ_i are the magnitude and phase of the field components in the axis i and K_g is a function of the geometry of the particle. For example in case of a spherical micro-object with a diameter r_2, K_g is expressed by:

$$K_g = 2\pi r_2^3 \quad (27)$$

The parameters K_{DEP} and K'_{DEP} is the real part and the imaginary part of the complex Clausius-Mosotti parameter. These parameters characterise the electric behavior of the particle and the medium and are expressed by:

$$K_{DEP} = Re\left(\frac{\kappa_2 - \kappa_3}{\kappa_2 + 2.\kappa_3}\right) \quad (28)$$

$$K'_{DEP} = Im\left(\frac{\kappa_2 - \kappa_3}{\kappa_2 + 2.\kappa_3}\right) \quad (29)$$

where
$\kappa_2 = \epsilon_2 - j\sigma_2/\omega$
$\kappa_3 = \epsilon_3 - j\sigma_3/\omega$
ϵ_2 : dielectric constant of the particle
ϵ_3 : dielectric constant of the medium
σ_2 : conductivity of the particle
σ_3 : conductivity of the medium
ω : angular freq. of the electric field

If the K_{DEP} parameter is positive, microparticle tends to move to the highest electric field gradient (near to the electrode). The dielectrophoretic force is attractive and is called 'positive-DEP'. In case of a negative K_{DEP}, microparticle tends to move to the lowest electric field (far from the electrode). The dielectrophoresis force is repulsive and is called 'negative-DEP'.

The dielectrophoresis (DEP) is usually used in cell micromanipulation to perform direct cell sorting [32][33] or field-flow-fractionation (FFF-DEP) [34][35]. In specific configurations, it allows to catch individual cells too [36]. Moreover dielectrophoresis is used to manipulate Carbon Nano Tubes (CNT) in the field of nanomanipulation [37]. Although this principle is not really effective in air, recently Subramanian presents first tests on the use of DEP in artificial objects manipulation in air [37]. In this medium, this kind of physical principle requires high voltage (eg. 200V).

Considering the submerged micro-objects manipulation is relevant and the DEP is particularly effective in liquid, we propose to apply this principle to submerged artificial micro-objects manipulation.

2) Robotic Micro-manipulation using Dielectrophoresis: The principle proposed is an original way to perform artificial micro-objects positioning. As the grasping by a gripper with two fingers allows to induce complex 3D trajectories and complex microassembly task (ie. insertion), we choose to manipulate micro-objects with a two fingers gripper. Consequently the

release task is perturbed by the adhesion force (pull-off force). We propose to use negative dielectrophoresis to control the micro-object release. Electric field could be produced by electrodes placed on the gripper or by using a conductive micro-gripper. After opening the gripper, an alternative electric field is applied on the gripper electrodes and induces a repulsive force on the micro-object whose objective is to release the object.

The behavior of the micro-object is composed of two phases:

- The micro-object is in contact with the gripper and is immobile (Fig 7(a)) .
- The micro-object is in motion in the liquid (Fig 7(b)) .

Before the release, forces applied to the micro-object is the adhesion force and the dielectrophoresis force. The release appears if the dielectrophoresis is greater than the pull-off force:

$$F_{DEP} > F_{PO} \tag{30}$$

After the release, in a very short time the micro-object reaches its maximum velocity. The micro-object trajectory is then defined by the equilibrium of the dielectrophoretic force and the hydrodynamic force F_{drag} induced by the liquid.

$$\overrightarrow{F}_{DEP} = -\overrightarrow{F}_{drag} \tag{31}$$

Consequently from (18) the trajectory of the particle is defined by its velocity $\overrightarrow{V}$:

$$\overrightarrow{V} = \frac{1}{k.\mu}\overrightarrow{F}_{DEP} \tag{32}$$

The transition (acceleration of the micro-object) between both cases is made in a very short time (ie. $50\mu s$) because of the small inertia of the micro-object. As the precise description of this acceleration phase has no specific interest in micromanipulation, the complete behavior of the micro-object is described by the equations (30-32).

3) Experimentations: To valid our approach, experimentations were performed on glass microsphere with a diameter $20\,\mu m$. The gripper is a four Degree Of Freedom (DOF) piezoelectric microgripper described in [38]. Specific end-effectors in Silicon were build with microfabrication technologies (D-RIE) and glued on the microgripper as presented in [38]. The silicon end-effectors and micro-gripper is presented in Figure 8. Thickness of the end-effectors is $12\,\mu m$ and the shape is presented in Figure 9. Gold electrodes are sputtered on the silicon end-effectors to applied alternating electric field.

An example of glass micro-sphere release is presented in Figure 9. The electric voltage used was a sinusoidal signal $\pm 20V$ peak-to-peak. The release and the trajectory of the micro-object is visible in Figure 9.

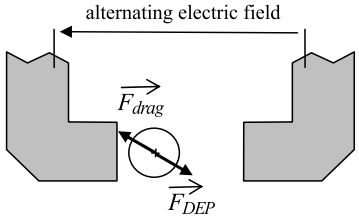

(a) First step: the dielectrophoretic force F_{DEP} overcome the pull-off force F_{PO}

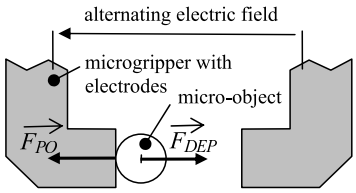

(b) Second step: the dielectrophoretic force F_{DEP} is opposed to drag force F_{drag}

Fig. 7. Principle of the dielectrophoretic release

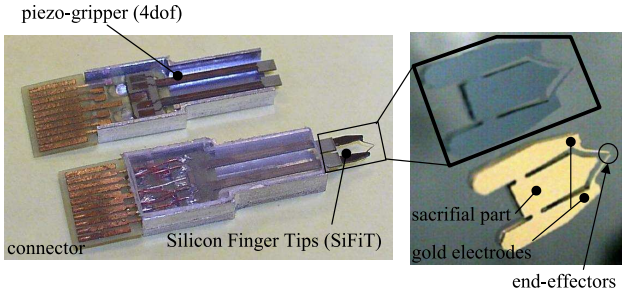

Fig. 8. Piezo-microgripper and Silicon Finger Tips (SiFiT)

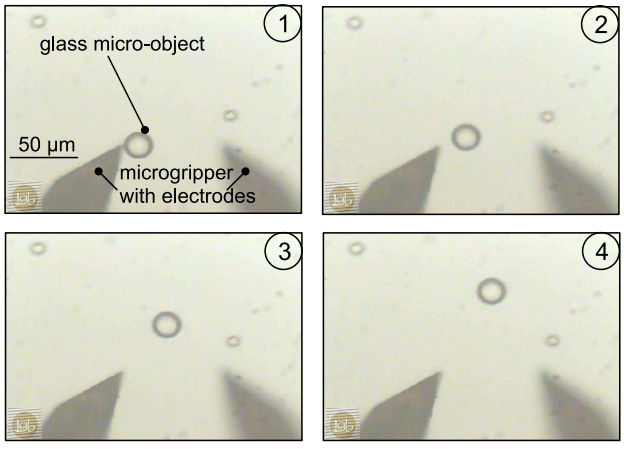

Fig. 9. Experimental DEP release

Experimentations show a high reliability on glass micro-object releases. The control of the release is easy to perform via the tension of electrodes. This first result demonstrates the interest in using dielectrophoresis release in submerged micromanipulations.

However at present, the final position of the released micro-object is not controlled. Further works will be done to purchase the modeling of the micro-object behavior after the release to control its final position. The shape, number, and architecture of electrodes will be studied and tested to optimize and control this release principle.

B. Submerged freeze gripper

This section is focused on the study of a submerged freeze microgripper. Its handling strategy is shown in Fig. 10. Firstly, the gripper comes close to the object without touching it. Secondly, an ice droplet is generated holding just a small part of the object. The object can be then picked and positioned. Finally, the ice droplet thaws mixing with the water and the object is released without any influence of capillary force.

As described below, the submerged freeze gripper utilizes the water environment to create an ice droplet. The cooling energy for freezing water is provided by two Peltier thermoelectric components.

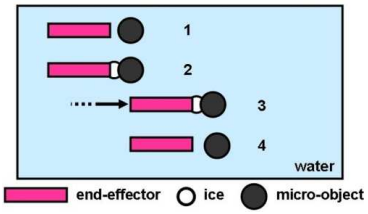

Fig. 10. Handling Strategy: (1) the micro-gripper approaches, (2) an ice droplet is generated and catches the object, (3) the object is manipulated, (4) the ice thaws and the object is liberated.

A Peltier module provides an electrical current-proportional generation or absorption of heat when direct current flows through it. The direction of the heat flow depends on the direction of the current, and the difference of temperatures caused by the heat transfer imposes two faces: a cold one and a hot one. The hot face must be associated to a heat sink in order to dissipate the heat flux.

As illustrated in Fig. 11, the submerged freeze system consists on two Peltier module stages, and a forced convection system. The first stage contains a Peltier micromodule named MicroPelt (μP). The end-effector is directly attached to its cold side. By this way, the MicroPelt can cool it and consequently generates the ice droplet on its acting part. The freezing process increases the temperature of the MicroPelt's hot face. Convection heat flow in water is thus so important than the whole system (liquid, gripper and Peltier micromodule) could warm up. To actively decrease the temperature at the MicroPelt's heat sink, a second Peltier element is connected. We called it MiniPeltier (mP). The temperature of its hot face must be constant to optimize its performance: it is maintained at the ambient temperature by forced convection using a liquid cooling system [39]. As MicroPelt's maximal cooling capacity is not sufficient to freeze the end-effector from ambient temperature, the liquid cooling system can not be used directly on its hot face.

The end-effector and the MicroPelt are completely submerged and electrically insulated. The MiniPeltier and the cooling liquid system stay in air to dissipate heat outside water.

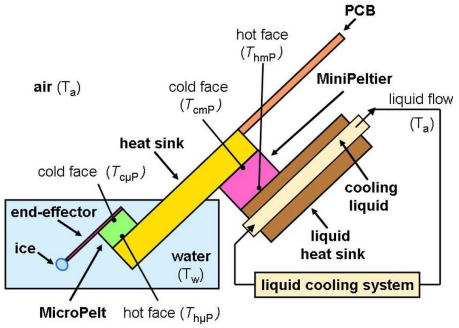

Fig. 11. Submerged Freeze System Principle.

1) Physical and Technical Characteristics: The first prototype of the submerged freeze gripper (without the end-effector) is shown in Fig. 12.

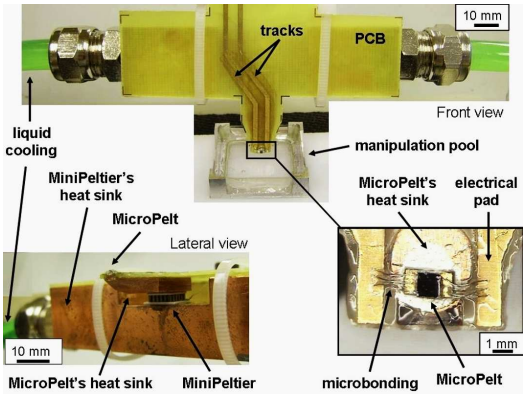

Fig. 12. Experimental freeze gripper.

The MicroPelt (Infineon Technologies AG) has as dimensions $720 \times 720 \times 428\ \mu m^3$. Its hot face is fastened to a copper heat sink (MicroPelt's heat sink). The MiniPeltier (Melcor FC0.6-18-05), which dimensions are $6.2 \times 6.2 \times 2.4\ mm^3$, is fixed on its cold face to the MicroPelt's heat sink; and on its hot face to the copper liquid heat sink of the cooling liquid system.

A specific PCB has been fabricated to establish the electrical connections of both Peltier modules. Because of the very small dimensions of the MicroPelt, microbonding technology were used for its connections.

2) First Experimentations: The first experimentations using the prototype described above were performed in distilled water at 2 ^{o}C. The objectives were to validate the good working of the system and its reliability. For these first tests, the end-effector was not included.

Fig. 13 describes the tele-manipulation of a silicon object whose dimensions are: 600 × 600 × 100 μm^3. A pre-cooling phase is necessary to decrease the temperature of the MicroPelt's heat sink. During this phase, only the current in the MiniPeltier (i_{mP}) is applied and set constant at 0.9 A (Fig. 13a). When the temperature is about 0.5 ^{o}C (this temperature is sufficiently close to 0 ^{o}C but it prevents the heat sink to freeze), the MicroPelt is approached to the micro-object and its current ($i_{\mu P}$) is turned on at 0.5 A. The cooling energy generates the ice droplet (4 μl) which involves a part of the object in 3 s (Fig. 13b). The freeze gripper can thus displace it towards a new position (Fig. 13c). To release it, the MicroPelt's current is inverted at -0.3 A. The ice droplet thaws in 7 s and melts with the aqueous medium, liberating the micro-object without adhesion perturbations (Fig. 13d). The micromanipulation has been performed in 30 s. As previously mentioned, the cycle time for pick and release, obtained for optimal working conditions of the Peltier modules, is $3 + 7 = 10$ s. The rest of the time, i.e. 20 s of transportation time in this case, depends principally on operator's ability, or microgripper speed in case of full automation. Contrary to the cryogenic grippers in air, capillary force does not perturb the release because the object and the MicroPelt are submerged. The Peltier currents choice is based on the thermal simulation presented in [40].

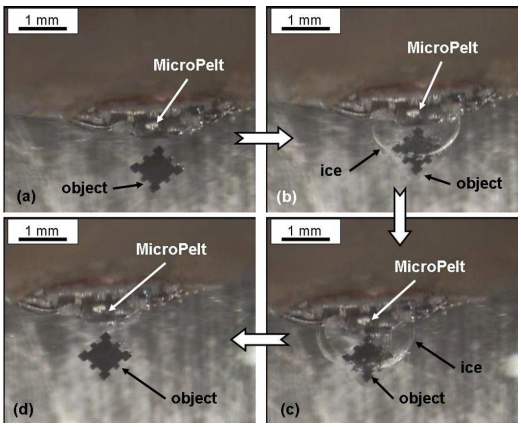

Fig. 13. Micromanipulation of a 600 × 600 × 100 μm^3 silicon object with the submerged freeze gripper.

The same experiment was successfully repeated several times. The submerged freeze principle seems thus a promising approach to manipulate micro-objects. Further manipulations will be dedicated to objects sized under 100 μm.

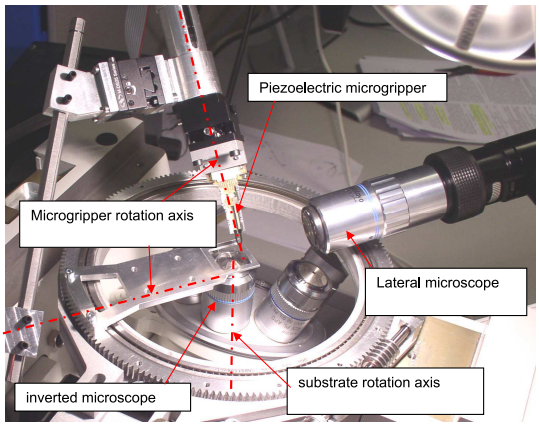

Fig. 14. 6 DOF robotic devices for micro-assembly

The thermal management becomes a crucial part of the microsystem design. However, thermal processes of the submerged freeze gripper involves combined heat conduction and convection leading to a complex system. The definition of a control strategy requires a model of the thermal exchanges in the whole system. The thermal modeling by electrical analogy is described in [39], [41].

V. Micro-assembly Platform

A. Platform Architecture

A 6 DOF (Degree Of Freedom) robotic platform has been build to perform complete microassembly tasks. An inverted microscope is used to visualized the micro-objects placed in a small pool (3cm square). The pool can be moved in the focus plane (2 translations and 1 rotation, see in figure 14). Thus each submerged objects can be positioned up to the microscope. A piezoelectric microgripper is placed on a 3 DOF robots which contains 2 rotations and 1 vertical translation (see in figure 14). A lateral microscope is used to visualize the vertical position. This view is only accessible in the air and not in liquid.

Only 4 DOF is currently used in teleoperation mode. Future works will focus on the geometrical modeling and the control of this structure to be able to use easily the 6 DOF.

B. Microassembly Application

The robotic platform is used to manipulate and to assembly micro-objects. Some silicon objects were build to produce microassembly benchmark. Objects is currently planar micro-objects as presented in figure 15. The silicon objects is build by using DIE etching in SOI wafers. After microfabrication, objects are linked to a millimetric silicon part through a breakable link.

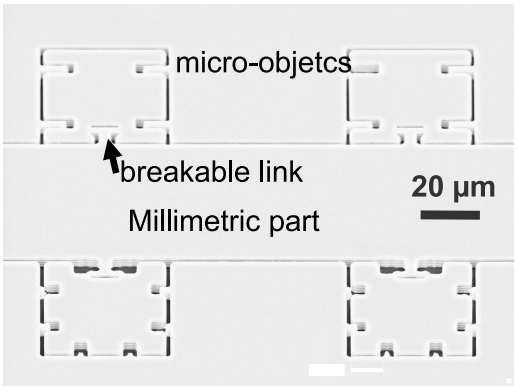

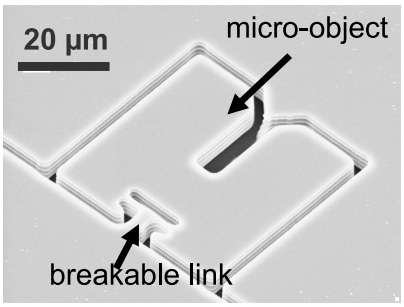

Fig. 15. Silicon Micro-objects to be assembled

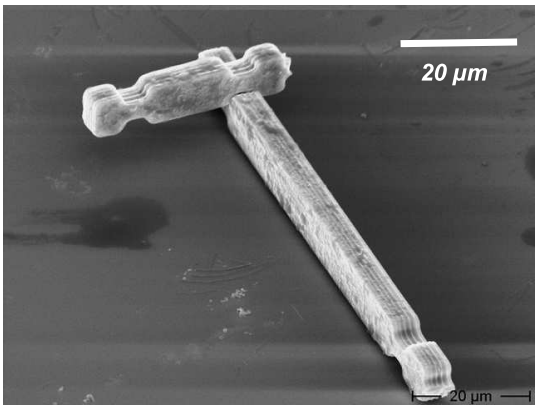

Fig. 16. Example of microassembly between to silicon tip

A first tool is used to break the link. During the release viscous forces are able to limit the micro-object velocity and avoid to loss the micro-object. The microgripper is then used to handle micro-object.

As the lateral view is not accessible for liquid micromanipulation, teleoperation in liquid is quite difficult and the current tests are performed in the air. The lack of vision access in liquid seems to be the major drawback to perform submerged microassembly. An example of microassembly of silicon parts is presented in figure 16.

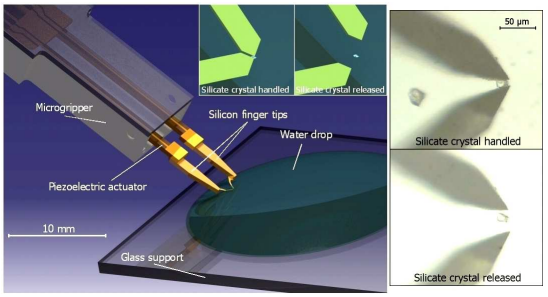

Fig. 17. Silicate crystal micromanipulation

C. Biological Application

Micromanipulation of artificial objects in a liquid has also applications in biological word. In particular, studying specific cells behavior in interaction with artificial objects could be used to determine their biocompatibility. In collaboration with the LST (Laboratoire de Sciences de la Terre, Lyon, France) a biological application has been chosen as a framework for the micro-manipulation station. Micro-sized particles of silicate have to be inserted in a liquid medium where E-Coli bacteria are living. Bacteria behavior around silicate particles will be studied with an inverted microscope. The applicative objective is to drop one silicate microcrystal near E-Coli bacteria in their liquid medium. Thus the micro-gripper was required to grasp one micro-crystal outside the liquid, bring it into and release it close to the biocells (see in figure 17) [42].

Conclusion

Development of new robotic micro-assembly methods and technologies is a keypoint to fabricate hybrid micro-systems as well as numerous micromechatronic products and requires reliable micromanipulation principles. At present, the release task is the most critical and unreliable phase because of the impact of the surface forces and adhesion forces. A complete modeling of the micro-forces in dry and liquid media was presented. These experiments exhibit a correlation better than 40% between the theoretical forces and the measured forces (except for pull-off in water). This theoretical and experimental comparative analysis between both types of medium shows the potential interest of the liquid in micromanipulation applications. In fact, contact and very large distance force are reduced in liquid while the hydrodynamic force significantly increases. Both phenomena are able to reduce respectively the electrostatic and adhesion perturbations and the loss of micro-objects. Furthermore, some submerged micromanipulation strategies (freeze gripper and dielectrophoretic gripper) are proposed. A 6 DOF robotic structure were build to perform complex trajectories for microassembly tasks. First results have demonstrate the microassembly capabilities of this platform. Further works will focus on the modeling of microforces in

function of the environment and on the automation of microassembly tasks.

References

[1] H. Van Brussel, J. Peirs, D. Reynaerts, A. Delchambre, G. Reinhart, N. Roth, M. Weck, and E. Zussman. Assembly of microsystems. *Annals of the CIRP*, 49(2):451–472, 2000.

[2] George M. Whitesides and Mila Boncheva. Beyond molecules: Self-assembly of mesoscopic and macroscopic components. *Proceedings of the National Academy of Sciences of the United States of America*, 99(8):4769–4774, 2002.

[3] T. Udeshi and K. Tsui. Assembly sequence planning for automated micro assembly. In *International Symposium on Assembly and Task Planning*, 2005.

[4] N. Dechev, W. L. Cleghorn, and J. K. Mills. Microassembly of 3d microstructures using a compliant, passive microgripper. *Journal of Microelectromechanical Systems*, 13(2), April 2004.

[5] R. Feynman. Infinitesimal machinery. *Journal of Microelectromechanical Systems*, 2, No 1:4–14, 1993.

[6] Y. Rollot, S. Regnier, and J-C. Guinot. Micro-robotics : A dynamical model of micro-manipulation by adhesion. In *Proc. of the Twelfth CISM-IFToMM Symposium, Theory and Practice of robots and manipulators, Paris, France , july*, pages 111–118, 1998.

[7] D.S. Haliyo and S. Régnier. Manipulation of micro-objects using adhesion forces and dynamical effects. In *Proceedings of ICRA/IEEE Internation Conferenace on Robotics and Automation*, May 2002.

[8] R.S. Fearing. A planar milli-robot system on air bearing. In *7th International Symp. Robotics Research*, HerrschingGermany, Oct. 1995.

[9] Q. Zhou, B. Chang, and H. N. Koivo. Ambient environment effects in micro/nano handling. In *Proc. of the Int. Workshop on Microfactories*, pages 146–51, Shangai, China, October 2004.

[10] R. Allen Bowling. A theoretical review of particle adhesion. In *Proc. of Symposium on particles on surfaces 1: Detection, Adhesion and Removal*, pages 129–142, San Francisco, 1986.

[11] J. Peirs. *Design of micromechatronic systems: scale laws, technologies, and medical applications*. PhD thesis, KUL, Belgium, 2001.

[12] M. Gauthier, S. Régnier, P. Rougeot, and N. Chaillet. Forces analysis for micromanipulations in dry and liquid media. *Journal of Micromechatronics*, 3(3-4):389–413, Sept. 2006.

[13] L.-H. Lee. The chemistry and physics of solid adhesion. In L.-H. Lee, editor, *Fundamentals of Adhesion*. Plenum Press, 1991.

[14] Y. Rollot. *Micro-manipulations par adhésion: Modélisations dynamiques et expérimentation*. PhD thesis, Université Pierre et Marie Curie, Paris, France, 2000.

[15] J. Israelachvili. *Intermolecular and Surface Forces*. Academic Press, 1991.

[16] Arthur W. Adamson and Alice P. Gast. *Physical Chemistry of Surfaces*. John Wiley and Sons, 6^{th} edition, 1997.

[17] A. McLachlan. Three-body dispersion forces. *Mol. Phys.*, 7:423–427, 1964.

[18] R. Allen Bowling. A theoretical review of particle adhesion. *ParticlesonSurfaces I*, 1988.

[19] Z. Xu and R. H. Yoon. The role of hydrophobic interactions in coagulation,. *J. Colloid Interface Sci.*, 44(132):532–541, 1989.

[20] Z. Xu and R.H. Yoon. A study of hydrophobic coagulation. *J. Colloid Interface Sci.*, 45(134):427–434, 1990.

[21] X-Y Lin, F. Creuset, and H. Arribart. Atomic force microscopy for local characterzation of surface acid-base properties. *J. Phys. Chem.*, 97:7272–76, 1993.

[22] Nehal I. Abu-Lail and Terri A. Camesano. Role of ionic strength on the relationship of biopolymer conformation, dlvo contributions, and steric interactions to bioadhesion of pseudomonas putida kt2442. *Biomacromolecules*, 4:1000–12, 2003.

[23] D. S. Rimai and D. J. Quesnel. *Fundamentals of Particle Adhesion*. Adhesion Society, 2001.

[24] M. Gauthier and M. Nourine. Capillary force disturbances on a partially submerged cylindrical micromanipulator. *IEEE Transactions on Robotics*, 23(3):600–604, Juin 2007.

[25] J.A. Greenwood K.L. Johnson. An adhesion map for the contact of elastic spheres. *J. Colloid Interface Sci.*, 192(2):326–333, 1997.

[26] B. V. Derjaguin, V.M. Muller, and YU. P. Toporov. effect of contact deformations on the adhesion of particles. *Journal of Colloid and interface science*, 53(2):314–326, 1975.

[27] Metin Sitti and Hideki Hashimoto. Teleoperated touch feedback from the surfaces at the nanoscale: Modelling and experiments. *IEEE-ASME Trans. Mechatron.*, 8(1):1–12, 2003.

[28] D. Maugis. Adhesion of spheres: the j.k.r-d.m.t transition using a dugdale model. *Journal of Colloid and Interface Science*, 150(1):243–269, 1992.

[29] M. Gauthier, B. Lopez-Walle, and C. Clévy. Comparison between micro-objects manipulations in dry and liquid mediums. In *proc. of CIRA'05*, June 2005.

[30] D. S. Haliyo and S. Régnier. Advanced applications using ţmad, the adhesion based dynamic micro-manipulator. In *Proceedings of the 2003 IEEE/ASME Int. Conf. on Advanced Intelligent Mechatronics (AIM 2003)*, pages 880–85, Port Island, Kobe, Japan, July 2003.

[31] P. Gascoyne, X. Wang, Y. Huang, and F. Becker. Dielectrophoretic separation of cancer cells from blood. In *IEEE Proc.*, pages 1366–1373, 1995.

[32] Frederick F. Becker, Peter R.C. Gascoyne, Ying Huang, and Xiao-Bo Wang. *Method and appartus for manipulation using spiral electrodes*. United States Patent, Patent Number US 5 858 192, 12 janv 1999.

[33] N. Tsukada, K. Kudoh, A. Yamamoto, T. Higuchi, M. Kobayashi, K. Sato, K. Oishi, and K. Iida. Development of oocyte rotation system for biological cell manipulation. In *Proc of the 32nd International Symposium on Robotics - ISR2001*, Seoul - Korea, 19-21 April 2001.

[34] P. Gascoyne and J. Vikoukal. Dielectrophoresis-based sample handling in general-purpose programmable diagnostic instruments. *IEEE Proceedings*, (1):22 – 42, 2004.

[35] M. Frenea, S. P. Faure, B. Le Pioufle, Ph. Coquet, and H. Fujita. Positioning living cells on a high-density electrode array by negative dielectrophoresis. *Materials Science and Engineering*, 23:597–603, 2003.

[36] A. Rosenthal and J. Voldman. Dielectrophoretic traps for single-particle patterning. *Biophysical Journal*, 88, march 2005.

[37] A Subramanian, B Vikramaditya, B J Nelson, D J Bell, and L Dong. Dielectrophoretic micro/nanoassembly with microtweezers and nanoelectrodes. In *Proc. of the 12th Int. Conf. on Advanced Robotics, Seattle*, July 2005.

[38] David Heriban, Joel Agnus, Jean-René Coudevylle, Michael Gauthier, and Nicolas Chaillet. Design of silicon finger tips for a moc (microrobot on chip) microgripper. In *Proc. of the Int. Workshop on Topica Meeting on Microfactories (TMMF05)*, Tsukuba, Japan, October 2005.

[39] B. Lopez Walle, M. Gauthier, and N. Chaillet. Dynamic modelling of a submerged freeze microgripper using a thermal network. In *proceedings of the 2007 IEEE/ASME International Conference on Advanced Intelligent Mechatronics*, sept. 2007.

[40] B.Lopez-Walle, M. Gauthier, and N. Chaillet. Submerged freeze gripper to manipulate micro-objects. In *proc. of the IEEE Int. Conf. on Intelligent Robots and Systems - IROS'06*, pages 784–789, Beijing, Chine,, oct. 2006.

[41] B. Lopez Walle, M. Gauthier, and N. Chaillet. A submerged freeze microgripper for micromanipulations. In *proc. of the 2007 IEEE International Conference on Robotics and Automation*, pages 10–14, Roma, Italy, April 2007.

[42] D Hériban, J Agnus, and M Gauthier. Micromanipulation of silicate micro-sized particles for biological applications. In *Proc. on the Int. Workshop on Microfactories*, Besancon, France, oct. 2006.